Continuous-Mode Hybrid Asymmetrical Load-Modulated Balanced Amplifier With Three-Way Modulation and Multi-Band Reconfigurability

Yuchen Cao, *Graduate Student Member, IEEE*, Haifeng Lyu, *Graduate Student Member, IEEE*, and Kenle Chen, *Senior Member, IEEE*

***Abstract*— This article introduces a novel high-order load modulation power amplifier (PA) architecture, i.e., continuous-mode hybrid asymmetric load modulated balanced amplifier (H-ALMBA). The two sub-amplifiers (BA1 and BA2) of the balanced topology in an LMBA are set as peaking amplifiers with different thresholds when cooperating with the control amplifier (CA) as the carrier, forming a hybrid load modulation behavior between Doherty and ALMBA. Compared to standard LMBA, the proposed H-ALMBA has a three-way load modulation with CA, BA1 and BA2 through proper amplitude control and phase alignment. Thus, this new mode offers extended power back-off range and enhanced back-off efficiency without suffering from difficulty and complexity in wideband design as imposed on three-way Doherty PAs. Based on comprehensive theoretical derivation and analysis, the proposed H-ALMBA is designed and implemented using commercial GaN transistors and wideband quadrature couplers. Moreover, the continuous-mode matching is applied to the carrier amplifier achieving a maximized wideband efficiency at power back-off. This is the first time that continuous mode and ALMBA have been used in combination, and very satisfactory results have been achieved, exhibiting the highest 10-dB OBO drain efficiency (DE) ever reported for wideband load-modulation PAs. The developed prototype experimentally demonstrates wide bandwidth from 1.7−3.0 GHz. The measurement exhibits an efficiency of 63−81% at peak output power, 51−62% for 5-dB OBO, and 50−66% for 10-dB OBO within the design bandwidth. When stimulated by a 20-MHz long term evolution (LTE) signal with 10.5-dB peak to average power ratio (PAPR), a 50−55% average efficiency is measured over the entire bandwidth at an average output power around 32 dBm.**

***Index Terms*— 5G, balanced amplifier, broadband, Doherty power amplifier, gallium nitride (GaN), high efficiency, reconfigurable.**

I. Introduction

With the rapid development of wireless ecosystem and advent of numerous emerging applications, the communications systems are demanded for supporting ever-growing data rates and user capacity. As a result, efficient use of spectrum resources has been a major priority for wireless network, which has triggered the wideband and complexly modulated communication signals with increasingly higher peak-to-average power ratio (PAPR). This, however, causes a dramatic degradation of average efficiency of power amplifier (PA), since it has to operate in significant power back-off most of the time. On the other hand, due to the rapid 4G/5G band proliferation, more and more spectrum fragments are being incorporated into wireless communications. In order to accommodate the ever-increasing number of allocated frequency bands, the RF bandwidth of power amplifiers and transmitters need to be as wideband as possible for accommodating multi-band communications without suffering from non-affordable hardware complexity, size, and cost. Therefore, developing broadband power amplifiers with enhanced back-off efficiency and high average efficiency has become an important proposition of this era.

Load modulation (LM) is one of the most compelling PA efficiency enhancement technologies. As a representative practical example, Doherty PA (DPA) has been widely employed in contemporary wireless communication infrastructures such as base stations due to its simplified topology and capability of effectively boosting back-off efficiency. However, the conventional DPA only offers a 6-dB output back-off (OBO) range, and the bandwidth is strongly limited by the quarter-wave inverters embedded in its generic circuit schematic. The extension of DPA bandwidth and OBO range has been intensively studied recently with substantial progresses, such as broadband asymmetric DPAs and multi-way DPAs [1]–[11]. Nevertheless, it is still very challenging to incorporate wideband matching techniques and high-efficiency PA modes (e.g., continuous Class-F/F^{-1} [12], [13]) into the Doherty design and meanwhile accurately control the load modulation, which prevents DPA from achieving the highest possible efficiency over a wide bandwidth. Another representative load-modulation PA, reverse-load-modulated dual branch (RMDB) PA [14], [15], has been proposed and demonstrated in recent years. However, RMDB PA is mostly used in MMIC implementation, and its peak and back-off efficiency still have certain gaps compared to DPA.

Recently, load modulated balanced amplifier (LMBA) has been proposed as a new high efficiency LM PA architecture [16]–[26]. It consists of a quadrature balanced

Manuscript received September 2, 2021; revised October 30, 2021; accepted November 13, 2021. Date of publication November 30, 2021; date of current version February 25, 2022. This work was supported in part by the National Science Foundation under Award 1914875. This article was recommended by Associate Editor J. Yin. *(Corresponding author: Kenle Chen.)*

The authors are with the Department of Electrical and Computer Engineering, University of Central Florida, Orlando, FL 32816 USA (e-mail: yuchencao@knights.ucf.edu; haifeng@knights.ucf.edu; kenle.chen@ucf.edu).

Color versions of one or more figures in this article are available at https://doi.org/10.1109/TCSI.2021.3129166.

Digital Object Identifier 10.1109/TCSI.2021.3129166

amplifier (BA) and a control amplifier (CA) with properly correlated amplitude and phase. This LMBA can be further designed with a Doherty type of biasing scheme with BA as carrier and CA as peaking, or vice versa. As presented in [27] and [28], we for the first time discovered that by setting the CA as carrier and BA as the peaking, a Doherty-like efficiency enhancement can be achieved with extended dynamic range and nearly unlimited bandwidth. This new mode is named pseudo-Doherty LMBA (PD-LMBA) in [28] and [29] or sequential LMBA in [30]. However, it is important to point out that the PD-LMBA as well as many of the variants of LMBA are technically a two-way modulation. With the increasing dynamic range of active load modulation, an undesired efficiency drop in the middle of the back-off levels becomes inevitable [19], [22], [30], [31]. To address this issue, this paper proposes a new high-order load-modulation platform based on the generic principle of asymmetrical LMBA (ALMBA) [23], and this new architecture is named hybrid ALMBA (H-ALMBA) [24]. The thresholds of the two transistors in the balanced amplifier are separated in this architecture, so that BA1 and BA2 are turned on sequentially, which can achieve three efficiency peaks throughout a larger OBO range. Meanwhile, the efficiency at the intermediate OBO level could be significantly enhanced. Compared with the three-way DPA with a general difficulty for wideband design, H-ALMBA perfectly inherits the wideband nature of PD-LMBA, since the same phase control condition is maintained.

Based upon the preliminary study in [24], the comprehensive theoretical derivation and analysis of H-ALMBA mode are presented in this paper for the first time. Moreover, we discovered that the continuous-mode matching with wideband harmonic tuning can be incorporated into the carrier amplifier (CA) design, and therefore, a high efficiency close to the theoretical limit of practical semiconductor devices can be achieved across the entire dynamic range with the cooperation of two peaking amplifiers (BA1 and BA2). Furthermore, a reciprocal biasing scheme with exchangeable turning-on sequence of peaking devices is proposed and adopted to maintain the optimal three-way load modulation behavior over the entire frequency range. The proposed theory, architecture, and design methodology are well validated with a practical prototype developed using GaN transistors and a wideband three-section branch-line quadrature hybrid as the output combiner.

II. Hybrid Asymmetrical LMBA Theory

The concept of H-ALMBA is developed from the recently reported LMBA [16], [23], [28], and it consists of three PAs, including a control amplifier (CA) biased in Class-AB mode, BA1 in Class-C mode, and BA2 in deep Class-C mode, as shown in Fig. 1(a). All PAs are connected to a 3-dB quadrature coupler with a port impedance of Z_0. The CA functions as the carrier amplifier, while BA1 and BA2 turn on sequentially at different OBO levels. When BA1 is turned on at low-back-off (LBO) level with BA2 remained off, CA and BA1 form a DPA-like PA. When BA2 is turned on at high-back-off (HBO) level, three PAs cooperate like the LMBA but

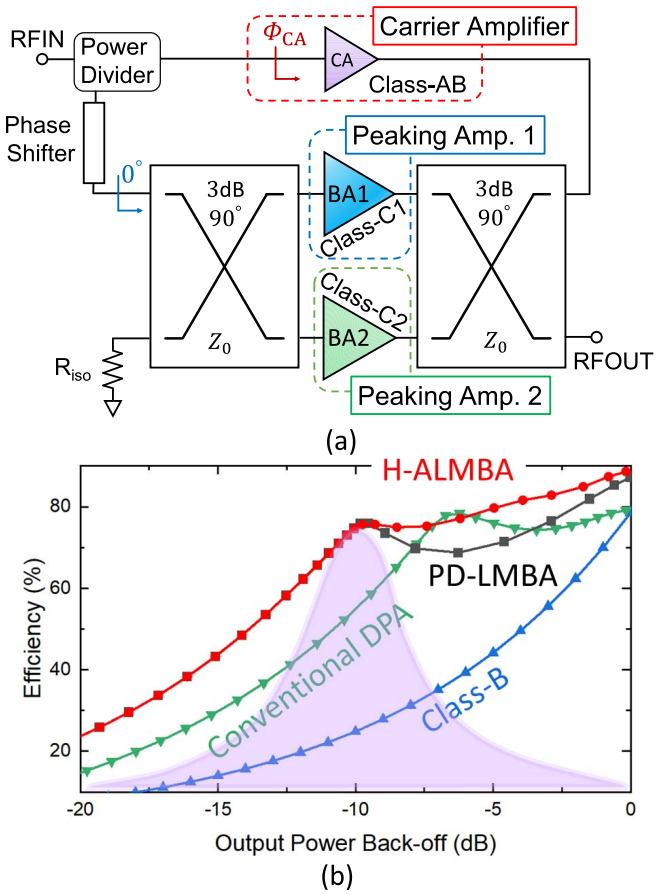

Fig. 1. H-ALMBA overview: (a) schematic and (b) simulated efficiency profile comparison between Class-B amplifier, conventional DPA, PD-LMBA, and H-ALMBA (simulation is based on bare-die GaN devices to emulate the ideal transistor models).

with BA1 and BA2 asymmetrical [23]. The load modulation of three amplifiers are different at different back-off ranges, which is similar to a three-way DPA. Therefore, multiple efficiency peaks can be formed across the extended dynamic power range, as plotted in red curve of Fig. 1(b), leading to a higher average efficiency when amplifying high-PAPR signals.

A. Generic Quadrature-Coupled Load Modulation

In the analytical modeling of H-ALMBA, all PAs are regarded as ideal voltage-controlled current sources, and they are coupled to the three ports of a 3-dB quadrature hybrid with the forth port connected to a load, as shown in Fig. 2. The voltages and currents of all four ports are dependent through the Z-matrix of quadrature coupler, expressed as

$$\begin{bmatrix} V_1 \\ V_2 \\ V_3 \\ V_4 \end{bmatrix} = Z_0 \begin{bmatrix} 0 & 0 & +j & -j\sqrt{2} \\ 0 & 0 & -j\sqrt{2} & +j \\ +j & -j\sqrt{2} & 0 & 0 \\ -j\sqrt{2} & +j & 0 & 0 \end{bmatrix} \begin{bmatrix} I_1 \\ I_2 \\ I_3 \\ I_4 \end{bmatrix} \quad (1)$$

where $V_1 = -I_1 Z_0$, $I_2 = I_{b1}$ and $I_4 = -jI_{b2}$ representing the input RF currents from BA1 and BA2, while $I_3 = jI_c e^{j\phi}$ denotes the CA current that is phase-shifted from BA1 by $\pi/2+\phi$ [16]. Using the matrix operation in (1), the impedances

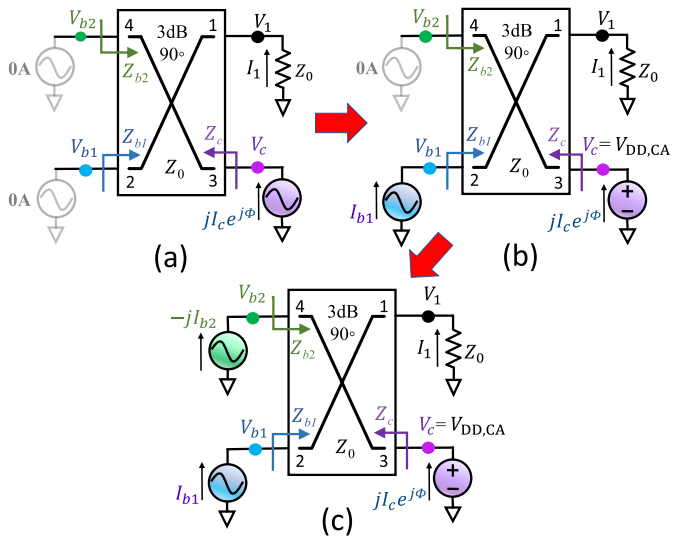

Fig. 2. Generalized schematic of quadrature-coupled three-way load modulation (H-ALMBA): (a) low-power region (CA only), (b) Doherty region (CA+BA1), (c) ALMBA region (CA+BA1+BA2).

of BA1, BA2 and CA can be calculated as

$$Z_{b1} = Z_0\left(\frac{I_{b2}}{I_{b1}} + \frac{\sqrt{2}I_c e^{j\phi}}{I_{b1}}\right); \tag{2}$$

$$Z_{b2} = Z_0\left(2 - \frac{I_{b1}}{I_{b2}} + \frac{\sqrt{2}I_c e^{j\phi}}{I_{b2}}\right); \tag{3}$$

$$Z_c = Z_0\left(1 - \sqrt{2}\frac{I_{b1} - I_{b2}}{I_c e^{j\phi}}\right). \tag{4}$$

Eqs. (2)-(4) indicate the generic quadrature-coupled load-modulation behavior [23], [24], which inclusively explains the original LMBA [16] and all its variants, e.g., [17], [26], [28], [30], [32]. Note that the load modulation of Z_{b1} and Z_{b2} can be controlled by the change of I_c amplitude and phase. At the same time, the load of carrier amplifier, Z_c, is determined by the difference between I_{b1} and I_{b2}. For standard ALMBA [23], the asymmetry between I_{b1} and I_{b2} is realized using different supply voltages ($V_{\mathrm{DD,BA1}}$, $V_{\mathrm{DD,BA2}}$), in order to control the load modulation of CA. In contrast, H-ALMBA leverages different turn-on thresholds of BA1 and BA2 ($V_{\mathrm{GS,BA1}}$, $V_{\mathrm{GS,BA2}}$), which can not only adjust I_{b1} and I_{b2} at different OBO levels but also form a three-way load modulation.

B. Modeling of Carrier and Peaking Generators

With different gate-bias settings of CA, BA1 and BA2, the dynamic operation of H-ALMBA can be divided into ***Low-Power*** (CA only), ***Doherty*** (CA+BA1), and ***ALMBA*** (CA+BA1+BA2) regions, illustrated in Figs. 2(a)-(c), respectively. To analyze the detailed load-modulation characteristics of H-ALMBA, the currents of all three amplifiers are carefully modeled [30].

As the carrier amplifier, the CA current, i_{ca}, is defined as

$$i_{\mathrm{ca}}(\beta) = \begin{cases} i_{\mathrm{ca,lp}}(\beta), & 0 \le \beta < \beta_{\mathrm{lbo}} \\ i_{\mathrm{ca,hp}}(\beta), & \beta_{\mathrm{lbo}} \le \beta \le 1 \end{cases} \tag{5}$$

where $i_{\mathrm{ca,lp}}$ is the CA current at low power region where the BA1 and BA2 are not turned on, and $i_{\mathrm{ca,hp}}$ denotes the

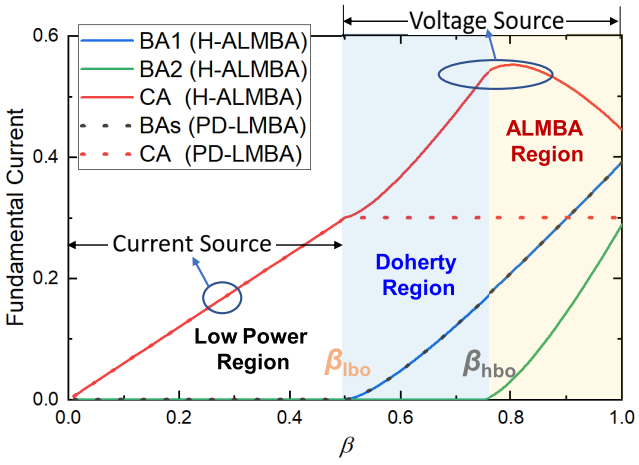

Fig. 3. Comparison of fundamental currents (normalized to $I_{\mathrm{Max,C/B}}$) of all three amplifiers in H-ALMBA and PD-LMBA modes.

CA current at high power region, including both Doherty and ALMBA regions. β is a normalized variable to describe the magnitude of the input driving level, and β_{lbo} is the BA1 threshold between the low-power region and DPA region. $i_{\mathrm{ca,lp}}$ can be simply expressed using the piece-wise linear model of standard Class-B mode:

$$i_{\mathrm{ca,lp}}(\beta) = \begin{cases} \beta I_{\mathrm{Max,C}} \cdot \cos\theta, & -\frac{\pi}{2} \le \theta < \frac{\pi}{2} \\ 0, & \text{otherwise} \end{cases} \tag{6}$$

where $I_{\mathrm{Max,C}}$ represents the maximum current allowed for the power device of CA. Using (6), the DC and fundamental components of $i_{\mathrm{ca,lp}}$ can be obtained as

$$i_{\mathrm{ca,lp}}[0] = \frac{\beta \cdot I_{\mathrm{Max,C}}}{\pi};$$
$$i_{\mathrm{ca,lp}}[1] = \frac{\beta \cdot I_{\mathrm{Max,C}}}{2}. \tag{7}$$

When the driving power increases to β_{lbo}, the CA must be saturated corresponding to the first efficiency peak at the target LBO level. For symmetrical PD-LMBA [27], [28], $i_{\mathrm{ca,lp}}$ grows to its maximum value, and this maximum CA current is maintained regardless of the continued increase of driving power towards the maximum input driving level, as the red dotted line plotted in Fig. 3. For H-ALMBA, however, only the voltage of CA is saturated at β_{lbo} that still leads to an efficiency peak. As β increases above β_{lbo}, the CA current continues to increase towards full saturation (both voltage and current) at $\beta = \beta_{\mathrm{hbo}}$, which is the BA2 threshold between the DPA region and ALMBA region, as shown in Fig. 3 (red solid line). For β between β_{hbo} and 1, the CA current can be subject to a decrease because the load impedance increases as BA2 turns on, indicated by (4), but the contribution of CA is overwhelmed by the two peaking amplifiers in this region. Nevertheless, it should be emphasized that the CA remains voltage-saturated offering a maximal efficiency across Doherty and ALMBA regions, and thus, in the high-power region, the modeling of CA is converted from a voltage-controlled current-source to an independent voltage source, which is no longer affected by the input voltage, as shown in Fig. 4. With

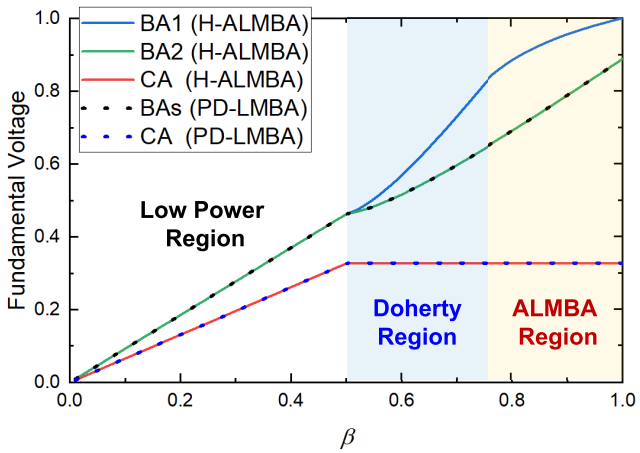

Fig. 4. Comparison of normalized fundamental voltages of each path in H-ALMBA and PD-LMBA mode.

a constant voltage saturation, the CA current can be expressed as

$$i_{\mathrm{ca,hp}}(\beta)=\begin{cases}\dfrac{2V_{\mathrm{DD,CA}}}{Z_c(\beta)}\cdot\cos\theta, & -\dfrac{\pi}{2}\le\theta<\dfrac{\pi}{2}\\ 0, & \text{otherwise}\end{cases}\tag{8}$$

where $V_{\mathrm{DD,CA}}$ equals to the maximum fundamental voltage of CA, and Z_c is the load impedance of CA that can be calculated from (4). As a voltage source, the CA fundamental voltage maintains a constant value of $V_{\mathrm{DD,CA}}$ as the red curve shown in Fig. 4. It is important to note that (8) is implicit, since $Z_c(\beta)$ is also dependent on the fundamental component of $i_{\mathrm{ca,hp}}$ as well as the currents of BA1 and BA2 in the high-power region, as indicated by (4). Thus, the CA current and load impedance in (8) will be eventually determined together with the BA1 and BA2 models. Particularly, the following boundary condition must be satisfied:

$$i_{\mathrm{ca,lp}}(\beta_{\mathrm{lbo}})=i_{\mathrm{ca,hp}}(\beta_{\mathrm{lbo}})\tag{9}$$

BA1 and BA2 are biased at Class-C mode with different thresholds. BA1 is turned on at β_{lbo}, while BA2 is turned on at β_{hbo}. The currents of BA1 and BA2 can be derived as

$$i_{\mathrm{ba1}}(\beta)=\begin{cases}0, & 0\le\beta<\beta_{\mathrm{lbo}}\\ i_{\mathrm{ba1,hp}}(\beta), & \beta_{\mathrm{lbo}}\le\beta\le 1\end{cases}\tag{10}$$

$$i_{\mathrm{ba2}}(\beta)=\begin{cases}0, & 0\le\beta<\beta_{\mathrm{hbo}}\\ i_{\mathrm{ba2,hp}}(\beta), & \beta_{\mathrm{hbo}}\le\beta\le 1\end{cases}\tag{11}$$

It should be noted that the peaking amplifier with full Class-C model is more precise and closer to realistic case, and most of the published LMBA articles adopt this method, e.g., [33], [34]. Therefore, the BA1 current in Doherty and ALMBA region can be expressed using Class-C current formula as

$$i_{\mathrm{ba1,hp}}(\beta)=\begin{cases}\dfrac{\beta\cdot\cos\theta-\beta_{\mathrm{lbo}}}{1-\beta_{\mathrm{lbo}}}I_{\mathrm{Max,B}}, & -\theta_b\le\theta<\theta_b\\ 0, & \text{otherwise}\end{cases}\tag{12}$$

$I_{\mathrm{Max,B}}$ represents the maximum current provided by the peaking device, which is assumed identical for BA1 and BA2. With a different turning-on threshold, the BA2 current in ALMBA region can also be expressed using Class-C current formula as

$$i_{\mathrm{ba2,hp}}(\beta)=\begin{cases}\dfrac{\beta\cdot\cos\theta-\beta_{\mathrm{hbo}}}{1-\beta_{\mathrm{hbo}}}I_{\mathrm{Max,B}}, & -\theta_b\le\theta<\theta_b\\ 0, & \text{otherwise}\end{cases}\tag{13}$$

where $(-\theta_b,+\theta_b)$ defines the turn-on phase range of BA1 and BA2. Thus, θ_b is obtained as

$$\theta_b=\arccos(\beta_{\mathrm{bo}}/\beta).\tag{14}$$

By applying Fourier Transformation, the DC and fundamental currents of BA1 and BA2 can be calculated as

$$\begin{aligned}i_{\mathrm{ba1,hp}}[0]&=\frac{I_{\mathrm{Max,B}}}{1-\beta_{\mathrm{lbo}}}\cdot\frac{\beta\sin\theta_b-\beta_{\mathrm{lbo}}\theta_b}{\pi};\\ i_{\mathrm{ba1,hp}}[1]&=\frac{I_{\mathrm{Max,B}}}{1-\beta_{\mathrm{lbo}}}\cdot\frac{\beta(2\theta_b+\sin2\theta_b)-4\beta_{\mathrm{lbo}}\sin\theta_b}{2\pi}.\end{aligned}\tag{15}$$

$$\begin{aligned}i_{\mathrm{ba2,hp}}[0]&=\frac{I_{\mathrm{Max,B}}}{1-\beta_{\mathrm{hbo}}}\cdot\frac{\beta\sin\theta_b-\beta_{\mathrm{hbo}}\theta_b}{\pi};\\ i_{\mathrm{ba2,hp}}[1]&=\frac{I_{\mathrm{Max,B}}}{1-\beta_{\mathrm{hbo}}}\cdot\frac{\beta(2\theta_b+\sin2\theta_b)-4\beta_{\mathrm{hbo}}\sin\theta_b}{2\pi}.\end{aligned}\tag{16}$$

Fig. 3 shows the normalized fundamental current of the BA1 and BA2 versus β with $\beta_{\mathrm{lbo}}=0.5$ and $\beta_{\mathrm{hbo}}=0.75$, respectively, and Fig. 4 depicts the corresponding voltages of BA1 and BA2. It is interesting to note that the voltage of individual BA in PD-LMBA ($\beta_{\mathrm{PD-LMBA}}=0.5$) is the same as that of BA2 in H-ALMBA.

C. Load Modulation Analysis of H-ALMBA

The detailed analysis on load-modulation behavior of H-ALMBA is performed for all three different regions:

- **Low-Power Region** ($P_{\mathrm{OUT}}<P_{\mathrm{MAX}}/\mathrm{LBO}$)**:** When operating at low power level below the predefined target LBO power, the BA1 and BA2 are not turned on, as depicted in Fig. 2(a). The CA operates as a standalone Class-B amplifier, and the output power is solely generated by CA. In this low-power region, there is no load modulation for all three amplifiers, and the currents are provided as following

$$\begin{aligned}I_c&=i_{\mathrm{ca,lp}}[1];\\ I_{b1}&=I_{b2}=0.\end{aligned}\tag{17}$$

  Their load impedances, $Z_{c,\mathrm{LP}}$, $Z_{b1,\mathrm{LP}}$, and $Z_{b2,\mathrm{LP}}$, can be expressed as

$$\begin{aligned}Z_{c,\mathrm{LP}}&=Z_0;\\ Z_{b1,\mathrm{LP}}&=Z_{b2,\mathrm{LP}}=\infty.\end{aligned}\tag{18}$$

  Since BA1 and BA2 (BAs) are not operating, the overall efficiency of H-ALMBA is equal to the efficiency of CA.
- **Doherty Region** ($P_{\mathrm{MAX}}/\mathrm{LBO}\le P_{\mathrm{OUT}}<P_{\mathrm{MAX}}/\mathrm{HBO}$)**:** When the output power increases to the target LBO level, BA1 is turned on, and CA reaches saturation at the same time. At $P_{\mathrm{MAX}}/\mathrm{LBO}$, CA is designed to be only voltage-saturated ($Z_c>Z_{\mathrm{CA,Opt}}$) corresponding to the first efficiency peak, while there is still headroom for

further increase of CA current. In this region, BA1 and CA currents both increases, given by

$$I_c = i_{\mathrm{ca,hp}}[1] = V_{\mathrm{DD,CA}}/Z_c;$$
$$I_{b1} = i_{\mathrm{ba1,hp}}[1]; \quad I_{b2} = 0. \tag{19}$$

By substituting the above currents into (2)-(4), and when $\phi = 0°$, the load modulation behaviors of CA, BA1, and BA2 impedances are derived as

$$Z_{c,\mathrm{Doherty}} = \frac{Z_0 V_{\mathrm{DD,CA}}}{V_{\mathrm{DD,CA}} + \sqrt{2} I_{b1} Z_0}|_{\phi=0°};$$
$$Z_{b1,\mathrm{Doherty}} = 2Z_0 + \frac{\sqrt{2} V_{\mathrm{DD,CA}}}{I_{b1}}|_{\phi=0°};$$
$$Z_{b2,\mathrm{Doherty}} = \infty. \tag{20}$$

The above equation clearly shows that as the power increases to the Doherty region, Z_c can be modulated below Z_0. Since the CA voltage remains constant ($=V_{\mathrm{DD,CA}}$) at this time, the current (I_c) and output power of CA can continue to increase.

- **ALMBA Region** ($P_{\mathrm{MAX}}/\mathrm{HBO} \leq P_{\mathrm{OUT}} < P_{\mathrm{MAX}}$)**:** When the driving power reaches β_{hbo}, BA2 is turned on, and the PA load modulation follows the ALMBA mode. Therefore, the currents of all three amplifiers can be expressed as

$$I_c = i_{\mathrm{ca,hp}}[1] = V_{\mathrm{DD,CA}}/Z_c; \tag{21}$$
$$I_{b1} = i_{\mathrm{ba1,hp}}[1]; \quad I_{b2} = i_{\mathrm{ba2,hp}}[1].$$

The load impedances of CA, BA1, and BA2 are can be described using (2)-(4), and when $\phi = 0°$, the impedance equations can be further derived as:

$$Z_{c,\mathrm{ALMBA}} = \frac{Z_0 V_{\mathrm{DD,CA}}}{V_{\mathrm{DD,CA}} + \sqrt{2}(I_{b1} - I_{b2}) Z_0}|_{\phi=0°};$$
$$Z_{b1,\mathrm{ALMBA}} = 2Z_0 + \frac{\sqrt{2} V_{\mathrm{DD,CA}} - Z_0 I_{b2}}{I_{b1}}|_{\phi=0°};$$
$$Z_{b2,\mathrm{ALMBA}} = \frac{Z_0 I_{b1} + \sqrt{2} V_{\mathrm{DD,CA}}}{I_{b2}}|_{\phi=0°}. \tag{22}$$

It could be observed from Fig. 3 that the fundamental current of BA2 increases more sharply as compared to the current of BA1. Thus, when the driving level (β) reaches to maximum, the BA1, BA2, and CA are all saturated respectively, and an maximum DE can be obtained.

Based on the above comprehensive load-modulation analysis, the load impedance and current of CA can be analytically determined using (4) and (8). The red curves (solid and dotted lines) in Fig. 5 compare the CA load modulation trajectories with $\phi = 0°$ between symmetrical PD-LMBA and H-ALMBA in different regions. Correspondingly, the overall fundamental CA current (I_c) versus driving level is plotted as the red curve in Fig. 3. The load modulation behaviors of BA1 and BA2 in H-ALMBA are calculated using (2)-(3), which are plotted in Fig. 5 in comparison with PD-LMBA. The normalized fundamental voltages of different amplifier branches in H-ALMBA and PD-LMBA modes are shown in Fig. 4.

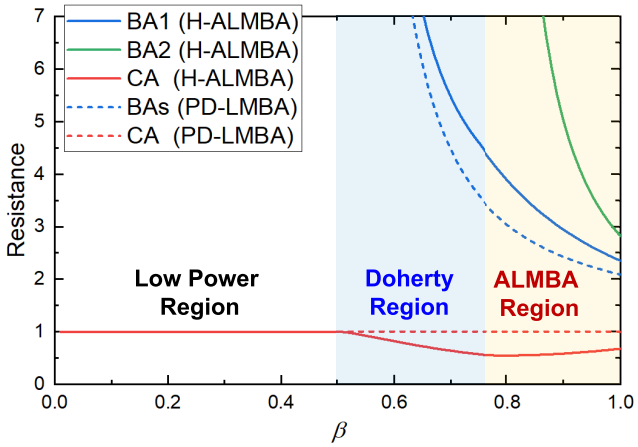

Fig. 5. Comparison of resistances of each path in H-ALMBA and PD-LMBA mode.

With the derived load modulation behaviors in terms of current, voltage, and impedance, the overall efficiency responses of PD-LMBA and H-ALMBA across the entire dynamic range are obtained and plotted as solid lines in Figs. 6(a) and (b), respectively, which also show the efficiencies of individual BA and CA. It can be seen that, in Doherty region (β from 0.5 to 0.75) with BA2 turned off, the BA efficiency of H-ALMBA increases more sharply than that of PD-LMBA. Therefore, an extra peak efficiency can be formed at the end of Doherty region (HBO level), which greatly improves the overall efficiency of the entire back-off range. Note that the efficiency at peak power is higher than 78.5% because of the Class-C operation of peaking amplifiers.

D. Amplitude and Phase Control of H-ALMBA

The amplitude control of H-ALMBA involves the power ratio of all three amplifiers and the turn-on points of BA1 and BA2. In this H-ALMBA operation, BA1 needs to be turned on at a pre-determined OBO level. By sweeping the turning on time of BA2, β_{hbo}, the optimal DE of the entire back-off region can be determined. The efficiency profiles with different β_{hbo} are shown in Fig. 7. It can be seen that the highest overall efficiency could be achieved with β_{hbo} between 0.7 and 0.8, which is close to half of the entire back-off region.

In addition to amplitude control, it is necessary to ensure that the phase difference between the power generators is properly set to result in optimal load modulation trajectories of each amplifier. As described in (20), by setting $\phi = 0°$, a purely resistive load modulation of Z_{b1}, Z_{b2}, Z_c can be achieved, which represent the optimal LM behaviors according to the classical load-line theory [35]. In realistic designs with matching networks and parasitics of transistors, the optimal BA-CA phase offset will be determined through exhaustive sweeping in the actual circuit schematic.

Moreover, compared to other load modulation architectures, H-ALMBA is easier to achieve different OBO levels by properly selecting the turning-on points of BA1 and BA2. The value of β_{lbo} not only represents the turning on point of BA1, but it also affects the selection of CA drain voltage, which can be utilized to ensure a voltage saturation of CA at the target

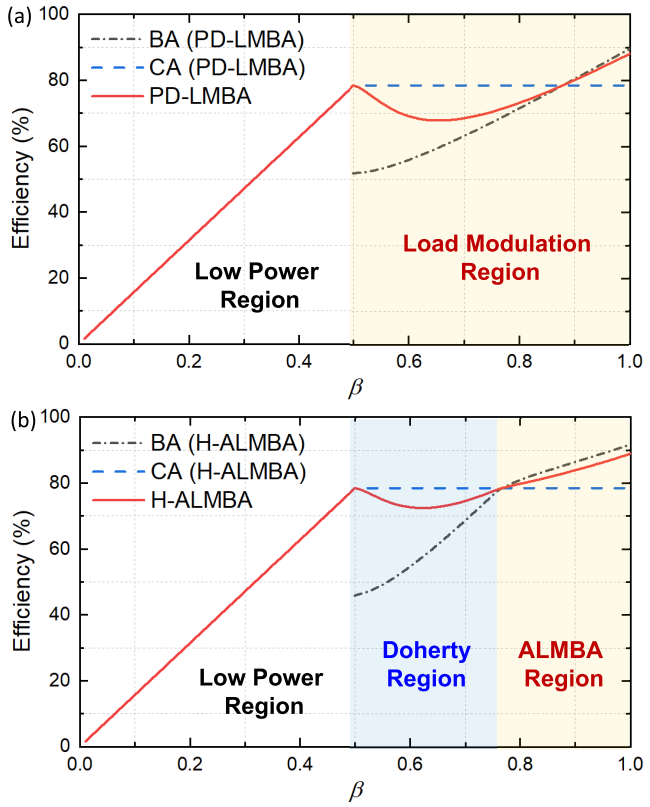

Fig. 6. Carrier and peaking efficiency performances: a) PD-LMBA; b) proposed H-ALMBA.

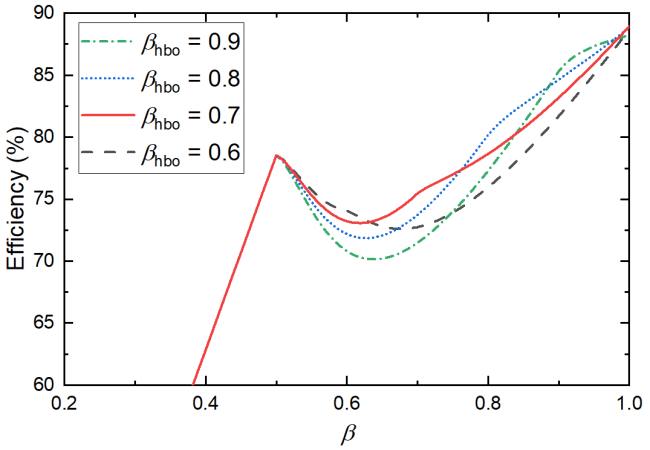

Fig. 7. Efficiency performance of the proposed H-ALMBA versus β with $\beta_{lbo} = 0.5$ and different values of β_{hbo}.

OBO. The β_{hbo} denotes the turning on of BA2, which can be leveraged to optimize the overall back-off efficiency for different OBO levels. Fig. 8 shows the efficiency performance of the proposed H-ALMBA with different β_{lbo} and β_{hbo}. Within the range from 0.6 to 0.2 of β_{lbo} and corresponding β_{hbo} from 0.75 to 0.45, the power back-off range of H-ALMBA could be extended from 7 dB to 17 dB with the highest possible back-off efficiency. The gain (AM-AM) profiles with different β_{lbo} and β_{hbo} are shown in Fig. 9. It can be seen that with the increase of the OBO range, a flatter gain response can be achieved. Overall, the efficiency and gain results indicate that the H-ALMBA mode is very suitable for amplification

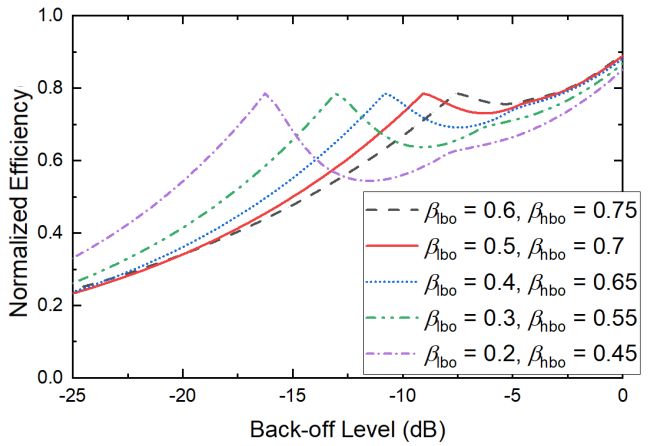

Fig. 8. Efficiency performance of the proposed H-ALMBA versus back-off level with different β_{lbo} and β_{hbo}.

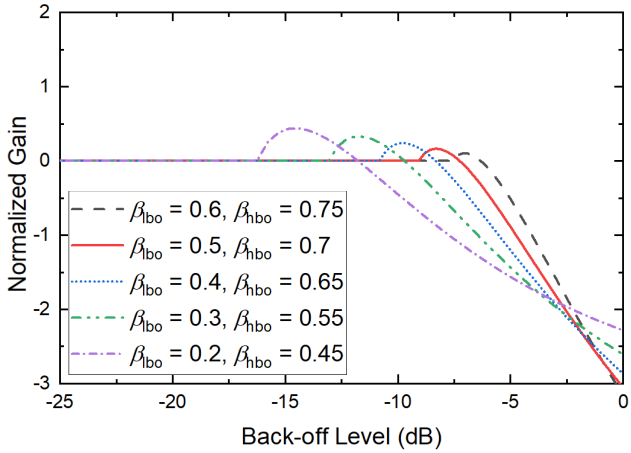

Fig. 9. Gain performance of the proposed H-ALMBA versus back-off level with different β_{lbo} and β_{hbo}.

of high-PAPR signals. It is worth noting in Fig. 9 that the change of β_{hbo} does not impact the gain response as long as β_{lbo} is fixed. This shows that even if the output power of CA is backed-off after BA2 is turned on (ALMBA region), it does not compromise the gain and power-added efficiency (PAE) of the overall PA.

E. Efficiency Enhancement of CA: Necessity and Approach

It should be noted that in the low-power region, the BA1 and BA2 are off, and all output power is generated by CA. Therefore, the impedance matching of the CA needs to ensure its wideband efficiency when operating alone, since the CA efficiency sets the first efficiency peak of the power back-off range and the average efficiency of entire PA. In the H-ALMBA architecture [23], CA is biased in Class-AB that has an efficiency naturally lower than that of the Class-B (78.5%). On the other hand, the CA output connects to the PA load through the output quadrature coupler, and the broadband output quadrature coupler itself usually has a certain internal loss. At the same time, when BA1 and BA2 are not turned on, BA1 and BA2 present off-state impedances to the corresponding ports of the output couplers, which can be regarded as two identical *R-C* tanks with the same quality factor (Q). The Q

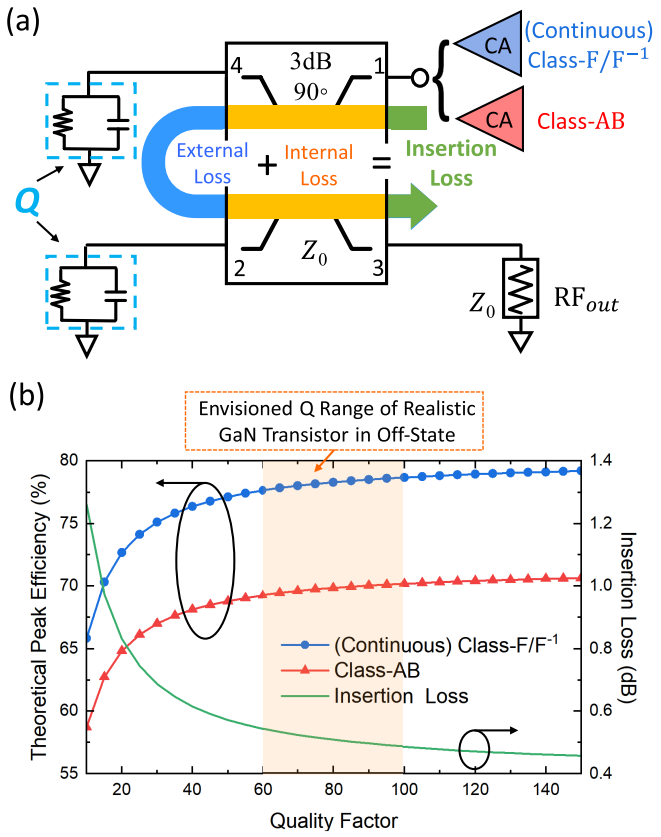

Fig. 10. Comparison of CA designed with continuous Class-F/F^{-1} and Class-AB: (a) schematic diagram; (b) ideal peak efficiency comparison with the same power loss.

of *R*-*C* tank determines the external power loss of quadrature coupler, which is added together with the internal loss forming the total insertion loss from CA port to the output, as shown in Fig. 10(a). Thus, the overall efficiency of CA in Class-AB mode can be significantly degraded, as the red curve depicted in Fig. 10(b).

In order to maximize the peak efficiency of CA, this paper combines the high-efficiency harmonic-tuned matching (e.g., Class-F/F^{-1} or its extension, continuous Class-F/F^{-1}) with H-ALMBA for the first time, and the output impedance matching with continuous mode (CM) is used to realize broadband CA design. Under the same insertion loss, the peak efficiency of the CA designed with continuous Class-F/F^{-1} (blue curve with circles) can be greatly improved as compared to that with Class-AB, as shown in Fig. 10(b) (the quadrature coupler internal loss is assumed to be 0.4 dB). Thus, upgrading CA from Class-AB to continuous Class-F/F^{-1} can greatly improve the peak efficiency of CA, thereby enhancing the overall PA back-off efficiency.

III. Practical Design of Ultra-Wideband Continuous-Mode H-ALMBA

In order to accommodate the high PAPR of emerging 5G and WiFi6 signals, the back-off range of the proposed H-ALMBA can be up to 17 dB according to actual needs, as shown in Fig. 8 and Fig. 9. In this design, a back-off range of 10-dB, is selected as a target OBO of this demonstrated work. The target frequency range is from 1.7 to 3.0 GHz, which could cover most cellular communication frequency bands.

A. Design of Control Amplifier in Continuous Mode

According to the amplitude control scheme described in Sec. II, the power of CA at the first efficiency peak determines the dynamic range once the output power of BA is fixed. Given a specific OBO target, the power of CA can be expressed by

$$\text{OBO} \times P_{\text{CA,Sat1}} = P_{\text{BA1,MAX}} + P_{\text{BA2,MAX}} + P_{\text{CA,Sat2}} \quad (23)$$

where $P_{\text{CA,Sat1}}$ represents the CA power at voltage saturation (first peak), and $P_{\text{CA,Sat2}}$ denotes the final CA power at maximum overall output power. A rough calculation indicates that $P_{\text{CA,Sat1}}$ is around 9-dB below $P_{\text{BA1,MAX}} + P_{\text{BA2,MAX}}$, while the accurate power dependence can be calculated by detailed analytical expressions presented in Sec. II. To realize this low output power, the CA is implemented with a 10-W GaN transistor (Wolfspeed CG2H40010), and it is biased in Class-AB mode with around 10-V drain bias voltage $V_{\text{DD,CA}}$. This value may be adjusted slightly at different frequencies to ensure that the OBO range of each frequency is 10 dB. It should be noted that this article is mainly targeted to verify the proposed H-ALMBA theory. Thus, for the convenience of fabrication, the same transistors are used in both CA and BAs. Since the CA power is much lower than BAs, it is physically realized using a lower V_{DD}. In realistic H-ALMBA design in MMIC, a smaller size of transistor can be designed for CA that is biased with the same V_{DD} as BAs, in order to avoid under-utilizing the CA device.

In low-power region, the BA1 and BA2 ports of the output coupler are open, and all output power is generated by CA. Therefore, in the actual matching design of the CA, the optimal wideband efficiency of CA standalone is considered, and meanwhile, its load modulation control of BA is also taken into account. However, a dilemma is envisioned: to ensure highest possible efficiency of standalone CA over the entire target bandwidth requires a complex harmonic-tuned wideband matching network, but an excessively complex matching network can cause uncontrollable phase dispersion [16] over frequency, which invalidates the precise phase control of BA. In [24], a simple three-segment transmission line is used as the output matching of the CA to maximize the efficiency of the BAs. But it also sacrifices the peak efficiency of CA, resulting in a reduction of the PA back-off efficiency.

In order to maximize the PA back-off efficiency, a simplified harmonic output matching network (OMN), similar to [36], is designed to realize a CM of CA for wideband operation, as shown in Fig. 11(a). Within the target frequency range from $1.7 - 3$ GHz, this OMN converts the Z_0 of isolation-port impedance of quadrature coupler to the fundamental impedance of continuous Class-F (CCF) and continuous Class-F^{-1} (CCF^{-1}) modes in the inductive half plane of Smith chart, as shown in Fig. 11(b). Meanwhile, the frequency response of this OMN over the second harmonic frequency range from $3.4 - 6$ GHz is distributed to the corresponding second harmonic impedance of the CCF^{-1} and CCF modes.

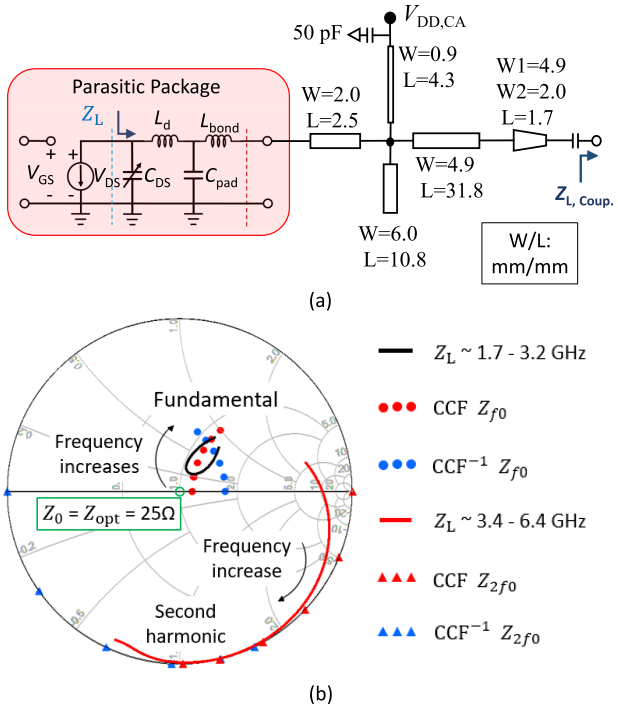

Fig. 11. OMN design of CA: (a) schematic of the designed CA-OMN with continue-mode; (b) simulated matching results of the designed CA-OMN from 1.7 to 3.0 GHz on the Smith chart with reference impedance.

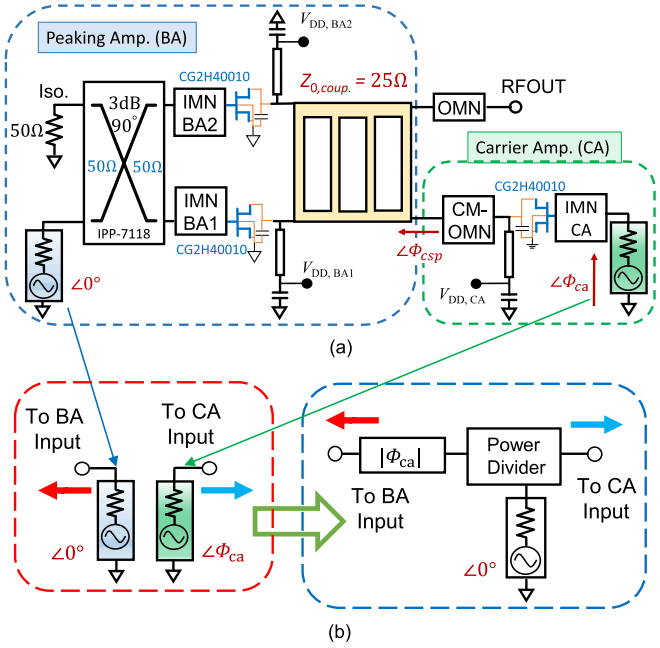

Fig. 12. (a) Simulation setup of the proposed H-ALMBA using realistic GaN transistors for verification and the transistor parasitic network, (b) design of TL-based wideband phase shifter for merging the BA and CA inputs.

Thus, a harmonic-tuned CA is realized in a transferring mode between CCF^{-1} and CCF.

On the other hand, the phase dispersion of this OMN is minimized since only one shunt stage (with a bias line and open-ended stub in parallel) is involved. The phase shift of series stages in the form of transmission lines (TLs) can be perfectly compensated with a phase offset line at BA input [28]. The wideband CA input-matching network (IMN) needs to ensure a decent gain performance within the target bandwidth. Therefore, a two-section lowpass network based on transmission lines is designed to provide wideband input matching for the selected GaN transistor.

B. Design of Balanced Amplifier With Asymmetrical Gate-Bias Setting

In this design, the two peaking amplifiers, i.e., BA1 and BA2, are designed with identical matching but different gate bias voltages. The input coupler (IPP-7118, available from Innovative Power Product [37]) is constructed using commercial equipment with a wide operating bandwidth of 1.7 to 3.0 GHz. The output coupler is realized with a non-50Ω three-stage branch hybrid structure, which can provide enough bandwidth to cover the design goal [38]. BA1 and BA2 are implemented with 10-W packaged GaN transistors (CG2H40010). Following the well demonstrated method in [23], [28], the BA output matching is performed using the characteristic impedance of output coupler ($Z_{0,\text{Coupler}}$) and bias lines (a shunt L). Note that the BA1 and BA2 are in Class-C mode, and their efficiencies are intrinsically higher than that of Class-B. Thus, the simplified matching of BA1 and BA2 suffices the harmonic tuning. It should also be noted that in the H-ALMBA design, load impedances of BA1 and BA2 are determined by the power (amplitude) and phase of CA, as indicated by (2) and (3). Therefore, the value of $Z_{0,\text{Coupler}}$ (= 25 Ω in this design) and the length of the bias lines are finalized through co-simulation with the CA using the simulation setup shown in Fig. 12(a).

A four-stage low-pass network is designed and implemented with transmission lines to provide input matching covering the target bandwidth from 1.7 to 3.0 GHz. Each stage consists of a series L (high impedance TL) and a shunt C (low impedance open stub). The length and width of TL are adjusted to absorb the parasitic effects of RF and DC modules and device packaging. The design of this matching circuit follows the widely adopted method introduced in [39].

C. Wideband BA-CA Phase Offset Design

The phase difference between BA1 and BA2 is fixed to 90° in a balanced amplifier. Therefore, after combining the complete BA (BA1 and BA2 with input and output couplers) and CA, the load modulation of all three amplifiers are mainly determined by the relative phase between BA and CA. In order to ensure the purely resistive load modulation of three amplifiers for maximized efficiency, a phase-adjustment network between BA and CA is required. Thus, an optimal phase offset is realized at the input of BA and CA, which can be determined using an equal-amplitude dual-input schematic diagram (similar to the method presented in [40]), as plotted in Fig. 12(b). By adding an ideal control signal to the isolation port of the output coupler, and scanning a large number of different phase values, the best phase corresponding to each frequency could be found. As shown in the red points of Fig. 13, the optimal phase shift between BA and CA is almost

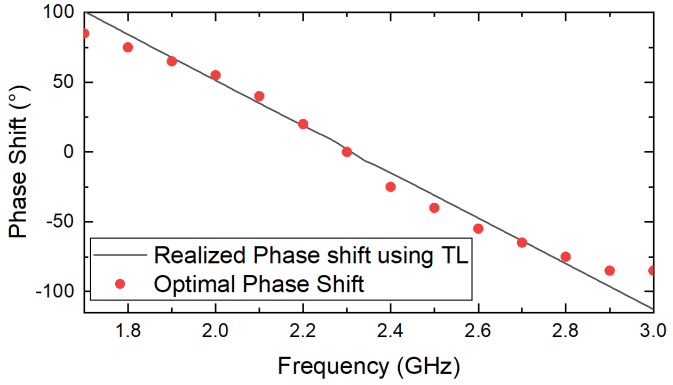

Fig. 13. Simulated optimal BA1-CA phase offset at different frequencies.

linearly proportional to the frequency with a negative slope. Therefore, an input-phase-adjustment network is added at the input side of BA by using a 50-Ω TL to suit the frequency-dependent phase-offset requirement [27]–[29]. The 'curve-fitting' results are plotted in Fig. 13. It can be seen that the realized TL phase shifter offers near-optimum phase setting at different frequencies. It should be noted that if the frequency continues to increase, the phase difference between BA and CA no longer completely comply to linear relationship, which could be due to the limited bandwidth of output quadrature coupler (i.e., three-section branch-line quadrature hybrid) and the phase dispersion of transistor parasitics. To further perfect the phase control over a broadened bandwidth, more precise phase control can be achieved through digital-assisted dual-input in the future designs.

It needs to be pointed out that, under ideal conditions, the CA impedance in the plane of the coupler isolation port should be Z_0 for any in band frequencies. Then, when BA1 is turned on, the CA impedance should be modulated to the lower impedance region, so that the CA output power can continue to increase, thus boosting the back-off efficiency, as the red curve shown in Fig. 14(a). However, due to the inevitable phase/amplitude imbalances of realistic broadband quadrature couplers, the load modulation of CA is affected as well as BA1 and BA2. Therefore, at some frequencies, the ideal turning on sequence does not lead to the desired back-off efficiency enhancement, e.g. 2.5 GHz of this design as the red curve shown in Fig. 14(b). Inspired by the reciprocal biasing scheme presented in [9], we can exchange the role of BA1 and BA2 with BA2 turned on first, in order to compensate the imperfects of quadrature coupler. At 2.5 GHz, the reciprocal biasing effective re-establishes the desired load modulation trajectory and the overall efficiency profile, as shown in the Fig. 14(b). With a combination of nominal and reciprocal biasing modes, the three-way load-modulation can be optimized over a wide bandwidth without having to rely on any additional tuning elements. This is an main advantage over the conventional three-way Doherty PA, which is difficult for wideband design.

D. Overall Schematic and Simulation Results

The designed final circuit schematic is shown in Fig. 15, and the values of all actual circuit elements are displayed next to the symbols. A 5-Ω resistor is added to the gate bias of each

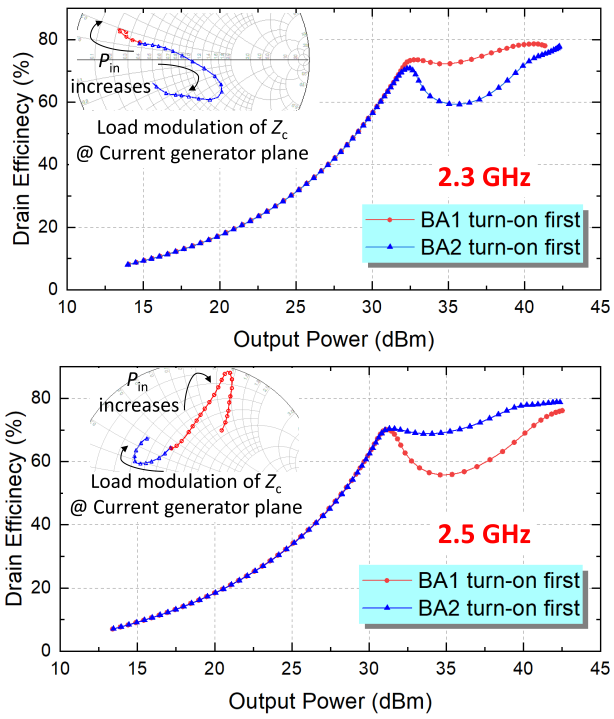

Fig. 14. Reciprocal turning-on sequence of BA1 and BA2 at different frequencies and its impact on CA load modulation and efficiency profile.

way and a parallel RC tank is added before the input matching network of BA1 and BA2 to ensure the stabilization of the entire PA. Between exchangeable gate biasing of BA1 and BA2 that is frequency-dependent, the first turning-on threshold is set to a gate bias voltage of −4.5 V, and the second one is set to −5.5 V. There are fine adjustments for different frequencies to ensure a LBO of 10-dB and a HBO of 5-dB could be obtained, where the CA load modulation is performed concurrently.

Through the design of the wideband BA1, BA2, CA, and phase shifter described in this section, the theoretical derivation results in section II have been perfectly verified by the simulation results, which are plotted in Fig. 16. Fig. 16(a) and (b) shows the simulated fundamental current and voltage at 2.2 GHz, respectively, and Fig. 16(c) depicts the load impedance trajectories of all three amplifiers at 2.2 GHz de-embedded to the intrinsic drain plane. The wideband drain efficiency and PAE of the designed H-ALMBA are simulated with swept input power, as shown in Fig. 17. It is clearly seen that a high efficiency of >70% is maintained from peak down to 10-dB back-off nearly across the entire frequency range. This is mainly due to the continuous-mode design of CA that ensures a high first efficiency peak and the effectiveness of the proposed H-ALMBA architecture.

IV. Implementation and Experimental Results

The overall layout is generated from circuit schematic, and it is electromagnetically modeled using ADS Momentum simulator. The proposed H-ALMBA is implemented on a 0.5-mm (20-mil) thick Rogers Duroid-5880 PCB board with a dielectric constant of 2.2. A photograph of the fabricated H-ALMBA is shown in Fig. 18. The size of the entire circuit

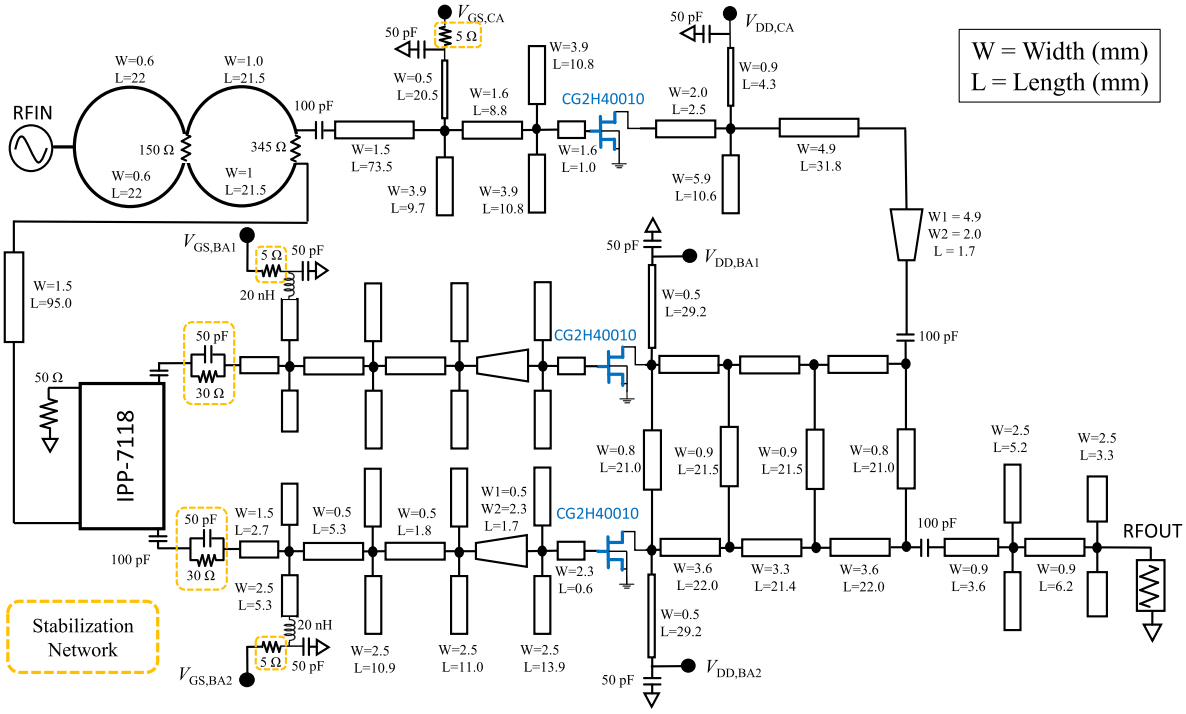

Fig. 15. Circuit schematic overview of designed CM-H-ALMBA.

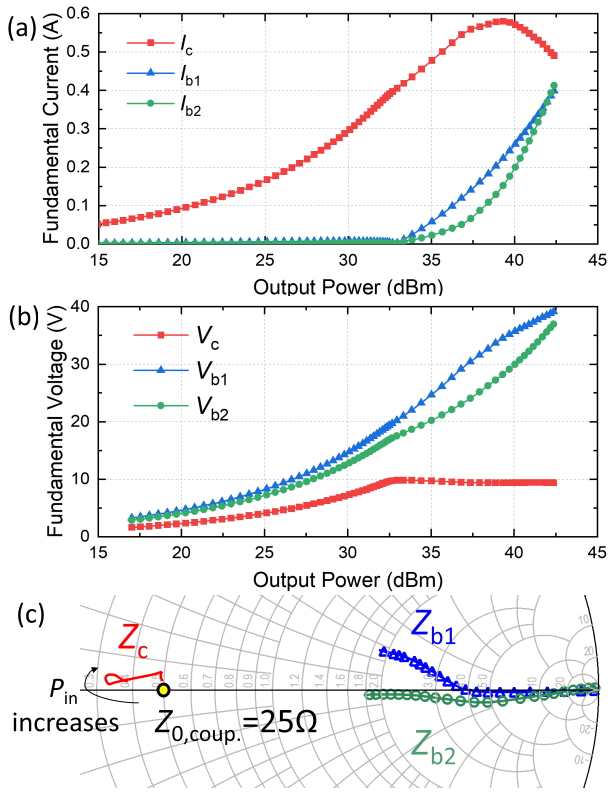

Fig. 16. Simulation results of the designed H-ALMBA at 2.25 GHz: (a) fundamental current; (b) fundamental voltage; (c) drain plane load trajectory.

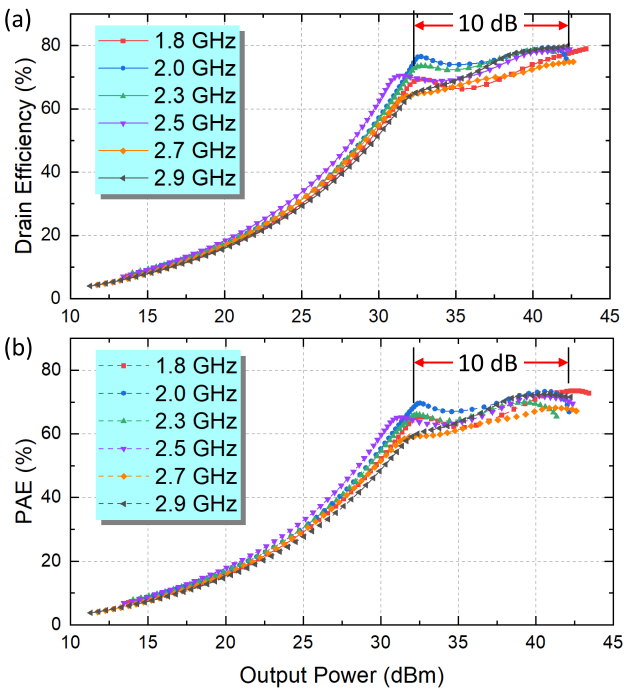

Fig. 17. Power-swept CW simulation results of the designed H-ALMBA with the best BA-CA phase setting at different frequencies: (a) drain efficiency; (b) PAE.

is 100 mm × 200 mm. The fabricated H-ALMBA is measured using both continuous-wave (CW) and modulated LTE signals. In this implemented circuit, the BA1 and BA2 are biased in Class-C with same 28-V V_{DD}. Based on different frequency, CA is biased in Class-AB with a $V_{DD,CA}$ range from 10 V to 13 V, which ensures CA saturation at 10-dB power back-off at all frequencies. The opening sequence of BA1 and BA2 is controlled by setting different V_{GS} bias voltages. The first opened BA V_{GS} is set at around −4.5 V, and the later opened BA V_{GS} is set at about −5.5 V. The value of $V_{GS,BA1}$ and $V_{GS,BA2}$ are adjusted to optimize the best PAE.

A. Continuous-Wave Measurement

The continuous-wave measurement is carried out with a CW power sweep inside the operating frequency band from

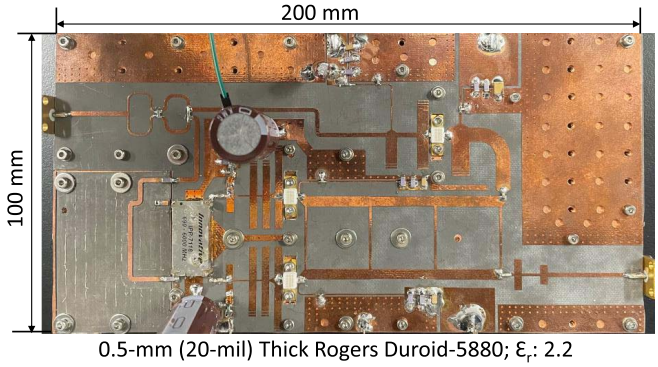

Fig. 18. Fabricated H-ALMBA prototype.

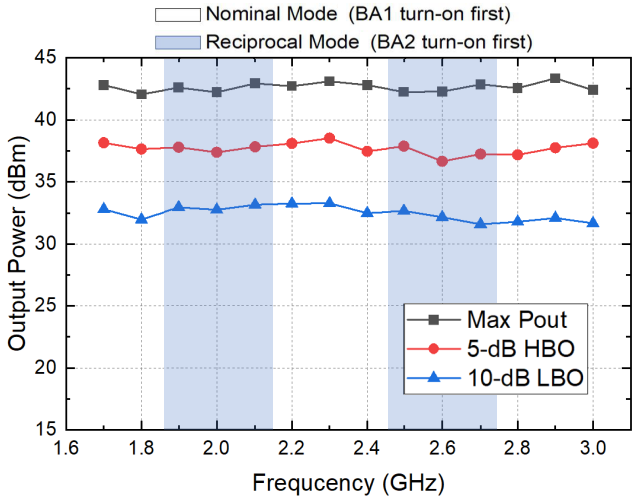

Fig. 19. Measured output power at various OBO levels from 1.7 to 3.0 GHz.

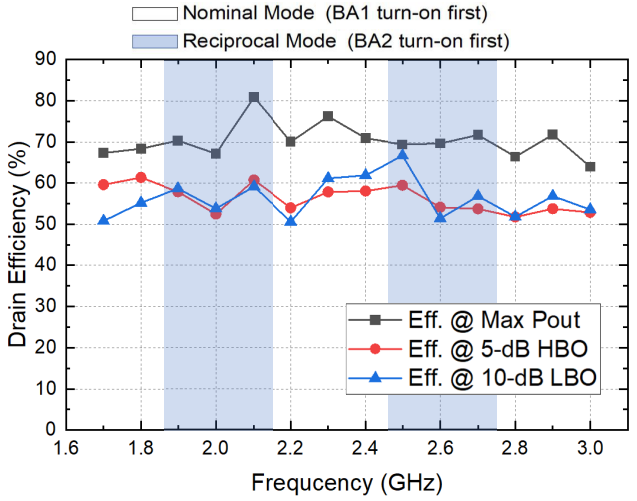

Fig. 20. Measured DE at various OBO levels from 1.7 to 3.0 GHz.

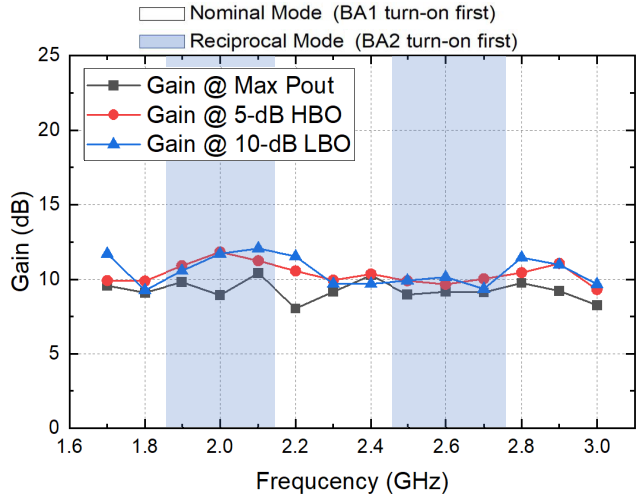

Fig. 21. Measured gain at various OBO levels from 1.7 to 3.0 GHz.

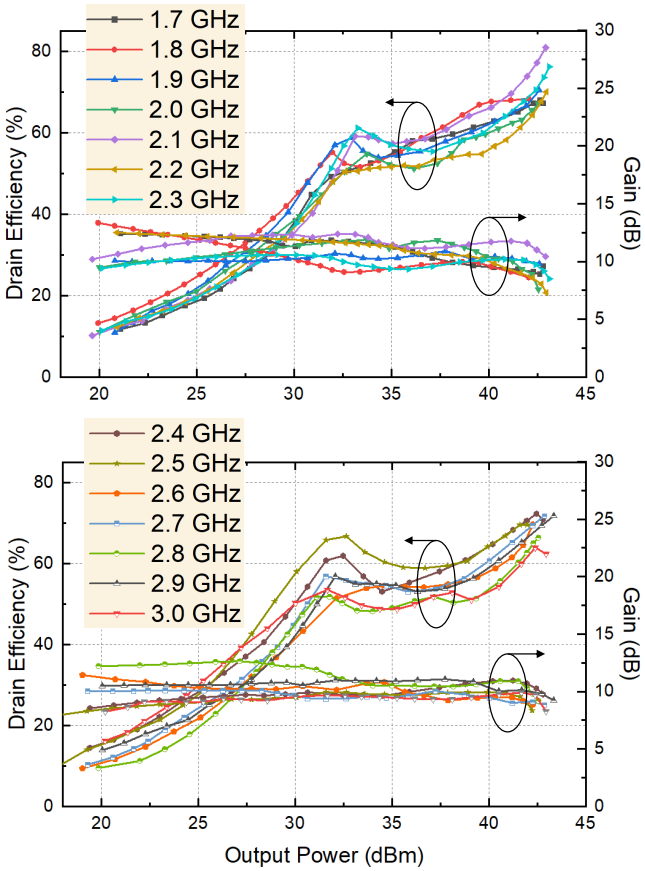

Fig. 22. Measured DE and gain versus output power from 1.7 to 3.0 GHz.

1.7 to 3.0 GHz. The CW signal is generated by a vector signal generator, and then boosted by a broadband linear driver amplifier to a sufficiently high level for driving the device under test (DUT). The output power is measured using power sensor and spectrum analyzer. As shown in Fig. 19, 42 – 43 dBm peak output power is measured across the entire bandwidth. As shown in Fig. 20, the maximum drain efficiencies at peak power are measured in the range of 63 – 81%, the drain efficiencies at 10-dB and 5-dB OBOs are in the range of 50 – 66% and 51 – 62%, respectively. It can be observed from Fig. 21 that the gain is maintained around 8 – 13 dB at different OBO level. Fig. 22 shows the measured drain efficiency and gain performance versus the output power. Fig. 23 is the PAE measurement performance versus the output power, which matches its theoretical results.

Two difference bias modes, nominal mode and reverse mode, are used in CW measurement to ensure the optimal efficiency performance. As shown in Fig. 19, Fig. 20, Fig. 21,

TABLE I
STATE-OF-THE-ART OF WIDEBAND LOAD-MODULATED POWER AMPLIFIERS

Ref. / Year	Architecture	Freq. (GHz)	FBW (%)	P_{Max} (dBm)	DE @ P_{Max} (%)	DE @ HBO (%)	DE @ LBO (%)
[4] 2018	3-Way DPA	2.0-2.6	26	43.6-45.4	53-76	46-58@5 dB*	41-48@8 dB
[5] 2019	3-Way DPA	1.6-2.6	48	45.5-46	53-66	47-57@5 dB*	50-53@9.5 dB
[41] 2018	3-Way DPA	0.6-0.9	40	46.1-46.9	51.1-78	54-65@5 dB*	42-64@9.5 dB*
[42] 2016	DPA	1.6-2.2	31.6	46-47	60-71	-	51-55@10 dB
[43] 2018	DPA	1.5-3.8	86.8	42.3-43.4	42-63	40-55@5 dB*	22-40@10 dB*
[44] 2019	DEPA	2.55-3.8	40	48.8-49.8	54-67	38-46@5 dB*	47-60@8 dB
[33] 2020	DPA	2.8-3.55	23.62	43-45	66-78	55-65@5 dB*	50-60.6@10 dB
[34] 2020	Dual-Mode DPA	1.52-4.68	102	41.5	54-71	45-60@5 dB*	37-50@10 dB*†
[18] 2017	RF-Input LMBA	0.7-0.85	19	42	57-70	-	30-35@10 dB*†
[40] 2017	RF-Input LMBA	1.8-3.8	71	44	46-70	30-51@5 dB*	20-25@10 dB*†
[45] 2018	Dual-Input LMBA	1.7-2.5	38	48-48.9	48-58*	38-46@5 dB*	33-45@10 dB*†
[28] 2020	PD-LMBA	1.5-2.7	57	43	58-72	48-60@5 dB	47-58@10 dB
[36] 2020	CM-LMBA	1.45-2.45	52	45.6-46.7	67.1-77.9	46-55@5 dB*	37-43@10 dB
[23] 2021	ALMBA	0.55-2.2	120	41-43	49-82	44-60@5 dB	39-64@10 dB
[24] 2021	H-ALMBA	0.55-2.2	120	42	55-82	51-69@5 dB	40-61@10 dB
This Work	H-ALMBA	1.7-3.0	55	42-43	63-81	51-62@5 dB	50-66@10 dB

* Graphically estimated, † PAE.

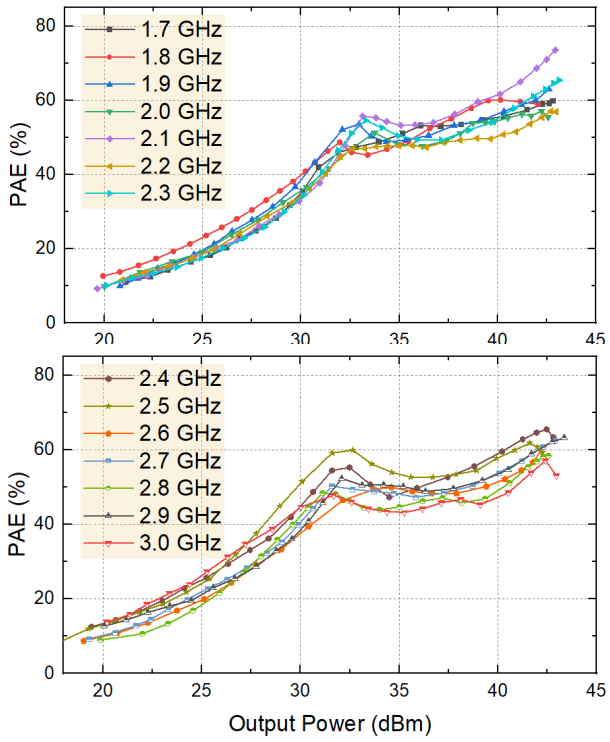

Fig. 23. Measured PAE versus output power from 1.7 to 3.0 GHz.

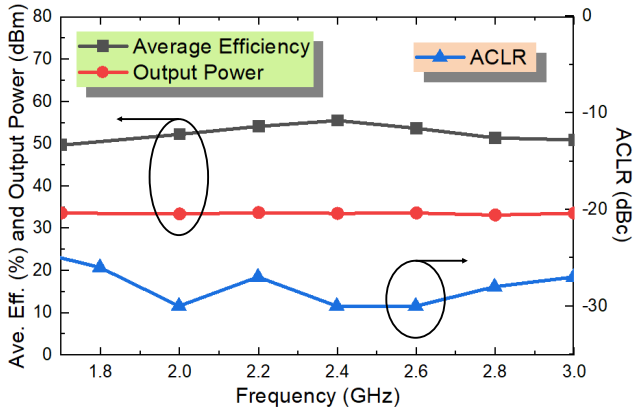

Fig. 24. Measured average DE, output power and ACLR with 20-MHz 9.5-dB-PAPR LTE signal at 1.7, 2.0, 2.2, 2.4, 2.6, 2.8 and 3.0 GHz.

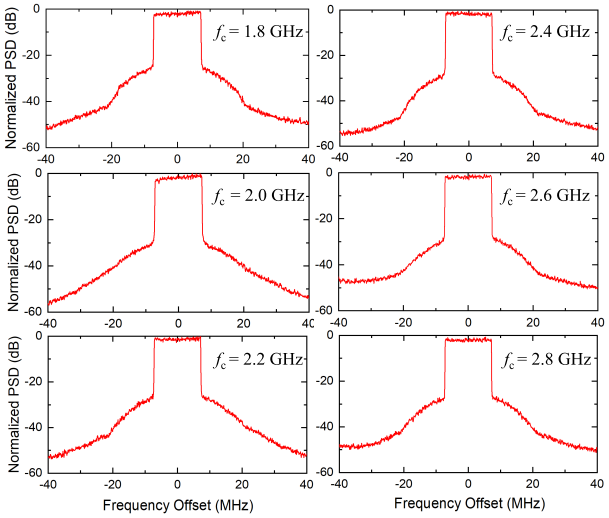

Fig. 25. Output spectrum from modulated measurement using a 20-MHz 9.5-dB-PAPR LTE signal centered at 1.8, 2.0, 2.2, 2.4, 2.6 and 2.8 GHz.

the white frequency interval is set to the nominal mode, where BA1 is turned-on first. And the blue frequency interval is set to reverse mode, where BA2 is turned-on first.

B. Modulated Measurement

To evaluate the linearity and efficiency performance of the proposed PA under modulated signal stimulation, 20-MHz LTE signals with 10-dB PAPR are used to test the proposed H-ALMBA at 1.7, 2.0, 2.2, 2.4, 2.6, 2.8 and 3.0 GHz. The modulated-signal is generated and analyzed by a Keysight PXIe vector transceiver (VXT M9421). The generated LTE signal is further boosted by a linear pre-amplifier (ZHL-5W-422+) to a sufficient level for driving the developed prototype. The measurement results at an average output power around 32 dBm are presented in Fig. 24. The H-ALMBA achieves a high average efficiency of 50% – 56% over the target frequency band. The ACLR of most measured frequencies are higher than 27 dB without any digital predistortion. Due to the load modulation of CA, the over-driving

issue of CA is greatly alleviated. As a result, the overall linearity of H-ALMBA has a better performance compared with PD-LMBA [28]. The measured output power spectral density (PSD) are shown in Fig. 25. The performance of the prototype PA is summarized and compared with other published works in Table I. This proposed H-ALMBA greatly enhances the entire back-off region efficiency down to 10-dB compared with the other LMBA architecture; while compared with the 3-way DPA, great advantage in ultra-bandwidth has been proved in the proposed H-ALMBA.

V. Conclusion

Based on the ALMBA theory, this paper proposes a new high-order load modulation mode, as well as its detailed design method and experimental validation. Through rigorous analysis and derivation, the design space of the load-modulation PA based on the quadrature coupler is further expanded with three-way modulation. In this new H-ALMBA mode, the asymmetry of the balanced amplifier is realized by setting different thresholds for BA1 and BA2, which leads to a hybrid load modulation combining a Doherty-like region (CA and BA1) and an ALMBA region (with all three amplifiers). As a result, a high-order load modulation can be formed like a three-way Doherty PA, resulting in an extended power back-off range and enhanced overall efficiency. Moreover, the H-ALMBA not only mitigates the CA over-driving issue in PD-LMBA but also inherits its wideband nature through proper phase alignment. The proposed theory and design method are experimentally verified using a developed hardware prototype, which is able to efficiently amplify the signals with 10-dB PAPR within a fractional bandwidth of 55%. This design greatly expands the design space of original LMBA and provides a promising solution for next generation multi-band and energy-efficient wireless transmitters.

References

[1] X. Zhou, S. Y. Zheng, W. S. Chan, S. Chen, and D. Ho, "Broadband efficiency-enhanced mutually coupled harmonic postmatching Doherty power amplifier," *IEEE Trans. Circuits Syst. I, Reg. Papers*, vol. 64, no. 7, pp. 1758–1771, Jul. 2017.

[2] H. Kang *et al.*, "Octave bandwidth Doherty power amplifier using multiple resonance circuit for the peaking amplifier," *IEEE Trans. Circuits Syst. I, Reg. Papers*, vol. 66, no. 2, pp. 583–593, Feb. 2019.

[3] H. Oh *et al.*, "Doherty power amplifier based on the fundamental current ratio for asymmetric cells," *IEEE Trans. Microw. Theory Techn.*, vol. 65, no. 11, pp. 4190–4197, Nov. 2017.

[4] S. Chen, W. Wang, K. Xu, and G. Wang, "A reactance compensated three-device Doherty power amplifier for bandwidth and back-off range extension," *Wireless Commun. Mobile Comput.*, vol. 2018, pp. 1–10, May 2018.

[5] J. Xia, W. Chen, F. Meng, C. Yu, and X. Zhu, "Improved three-stage Doherty amplifier design with impedance compensation in load combiner for broadband applications," *IEEE Trans. Microw Theory Techn.*, vol. 67, no. 2, pp. 778–786, Feb. 2019.

[6] Y. Cao, H. Lyu, and K. Chen, "Wideband Doherty power amplifier in quasi-balanced configuration," in *Proc. IEEE 20th Wireless Microw. Technol. Conf. (WAMICON)*, Apr. 2019, pp. 1–4.

[7] H. Lyu, Y. Cao, and K. Chen, "Doherty-to-balanced switchable power amplifier," in *IEEE MTT-S Int. Microw. Symp. Dig.*, Jun. 2019, pp. 1339–1342.

[8] H. Lyu and K. Chen, "Balanced-to-Doherty mode-reconfigurable power amplifier with high efficiency and linearity against load mismatch," *IEEE Trans. Microw. Theory Techn.*, vol. 68, no. 5, pp. 1717–1728, Mar. 2020.

[9] H. Lyu, Y. Cao, and K. Chen, "Linearity-enhanced quasi-balanced Doherty power amplifier with mismatch resilience through series/parallel reconfiguration for massive MIMO," *IEEE Trans. Microw. Theory Techn.*, vol. 69, no. 4, pp. 2319–2335, Apr. 2021.

[10] C. Liang, P. Roblin, Y. Hahn, Z. Popovic, and H.-C. Chang, "Novel outphasing power amplifiers designed with an analytic generalized Doherty–Chireix continuum theory," *IEEE Trans. Circuits Syst. I, Reg. Papers*, vol. 66, no. 8, pp. 2935–2948, Aug. 2019.

[11] C. Li, F. You, S. He, X. Tang, W. Shi, and J. Wang, "High-efficiency power amplifier employing minimum-power harmonic active load modulator," *IEEE Trans. Circuits Syst. II, Exp. Briefs*, vol. 66, no. 8, pp. 1371–1375, Aug. 2019.

[12] V. Carrubba *et al.*, "On the extension of the continuous class-F mode power amplifier," *IEEE Trans. Microw. Theory Techn.*, vol. 59, no. 5, pp. 1294–1303, May 2011.

[13] K. Chen and D. Peroulis, "Design of broadband highly efficient harmonic-tuned power amplifier using in-band continuous class-F^{-1}/F mode transferring," *IEEE Trans. Microw. Theory Techn.*, vol. 60, no. 12, pp. 4107–4116, Dec. 2012.

[14] M. Akbarpour, F. M. Ghannouchi, and M. Helaoui, "Current-biasing of power-amplifier transistors and its application for ultra-wideband high efficiency at power back-off," *IEEE Trans. Microw. Theory Techn.*, vol. 65, no. 4, pp. 1257–1271, Apr. 2017.

[15] Y. Zhao *et al.*, "Theory and design methodology for reverse-modulated dual-branch power amplifiers applied to a 4G/5G broadband GaN MMIC PA design," *IEEE Trans. Microw. Theory Techn.*, vol. 69, no. 6, pp. 3120–3131, Jun. 2021.

[16] D. J. Shepphard, J. Powell, and S. C. Cripps, "An efficient broadband reconfigurable power amplifier using active load modulation," *IEEE Microw. Wireless Compon. Lett.*, vol. 26, no. 6, pp. 443–445, Jun. 2016.

[17] D. J. Shepphard, J. Powell, and S. C. Cripps, "A broadband reconfigurable load modulated balanced amplifier (LMBA)," in *IEEE MTT-S Int. Microw. Symp. Dig.*, Jun. 2017, pp. 947–949.

[18] P. H. Pednekar and T. W. Barton, "RF-input load modulated balanced amplifier," in *IEEE MTT-S Int. Microw. Symp. Dig.*, Jun. 2017, pp. 1730–1733.

[19] D. Collins, R. Quaglia, J. Powell, and S. Cripps, "Experimental characterization of a load modulated balanced amplifier with simplified input power splitter," in *Proc. Asia–Pacific Microw. Conf. (APMC)*, Nov. 2018, pp. 461–463.

[20] T. Cappello, P. Pednekar, C. Florian, S. Cripps, Z. Popovic, and T. W. Barton, "Supply- and load-modulated balanced amplifier for efficient broadband 5G base stations," *IEEE Trans. Microw. Theory Techn.*, vol. 67, no. 7, pp. 3122–3133, Jul. 2019.

[21] H. Jeon *et al.*, "A triple-mode balanced linear CMOS power amplifier using a switched-quadrature coupler," *IEEE J. Solid-State Circuits*, vol. 47, no. 9, pp. 2019–2032, Sep. 2012.

[22] T. Cappello, P. H. Pednekar, C. Florian, Z. Popovic, and T. Barton, "Supply modulation of a broadband load modulated balanced amplifier," in *IEEE MTT-S Int. Microw. Symp. Dig.*, Jun. 2018, pp. 304–307.

[23] Y. Cao, H. Lyu, and K. Chen, "Asymmetrical load modulated balanced amplifier with continuum of modulation ratio and dual-octave bandwidth," *IEEE Trans. Microw. Theory Techn.*, vol. 69, no. 1, pp. 682–696, Jan. 2021.

[24] Y. Cao and K. Chen, "Hybrid asymmetrical load modulated balanced amplifier with wide bandwidth and three-way-Doherty efficiency enhancement," *IEEE Microw. Wireless Compon. Lett.*, vol. 31, no. 6, pp. 721–724, Jun. 2021.

[25] H. Lyu and K. Chen, "Hybrid load-modulated balanced amplifier with high linearity and extended dynamic range," *IEEE Microw. Wireless Compon. Lett.*, vol. 31, no. 9, pp. 1067–1070, Sep. 2021.

[26] Y. Xu, J. Pang, X. Wang, and A. Zhu, "Three-stage load modulated power amplifier with efficiency enhancement at power back-off," *IEEE Trans. Microw. Theory Techn.*, vol. 69, no. 6, pp. 3107–3119, Jun. 2021.

[27] Y. Cao, H. Lyu, and K. Chen, "Load modulated balanced amplifier with reconfigurable phase control for extended dynamic range," in *IEEE MTT-S Int. Microw. Symp. Dig.*, Jun. 2019, pp. 1335–1338.

[28] Y. Cao and K. Chen, "Pseudo-Doherty load-modulated balanced amplifier with wide bandwidth and extended power back-off range," *IEEE Trans. Microw. Theory Techn.*, vol. 68, no. 7, pp. 3172–3183, Jul. 2020.

[29] Y. Cao and K. Chen, "Dual-octave-bandwidth RF-input pseudo-Doherty load modulated balanced amplifier with $\geq$ 10-dB power back-off range," in *IEEE MTT-S Int. Microw. Symp. Dig.*, Aug. 2020, pp. 703–706.

[30] J. Pang *et al.*, "Analysis and design of highly efficient wideband RF-input sequential load modulated balanced power amplifier," *IEEE Trans. Microw. Theory Techn.*, vol. 68, no. 5, pp. 1741–1753, Jan. 2020.

[31] G. R. Nikandish, R. B. Staszewski, and A. Zhu, "Unbalanced power amplifier: An architecture for broadband back-off efficiency enhancement," *IEEE J. Solid-State Circuits*, vol. 56, no. 2, pp. 367–381, Feb. 2021.

[32] P. H. Pednekar, W. Hallberg, C. Fager, and T. W. Barton, "Analysis and design of a Doherty-like RF-input load modulated balanced amplifier," *IEEE Trans. Microw. Theory Techn.*, vol. 66, no. 12, pp. 5322–5335, Dec. 2018.
[33] M. Li, J. Pang, Y. Li, and A. Zhu, "Bandwidth enhancement of Doherty power amplifier using modified load modulation network," *IEEE Trans. Circuits Syst. I, Reg. Papers*, vol. 67, no. 6, pp. 1824–1834, Jun. 2020.
[34] J. Pang, Z. Dai, Y. Li, M. Li, and A. Zhu, "Multiband dual-mode Doherty power amplifier employing phase periodic matching network and reciprocal gate bias for 5G applications," *IEEE Trans. Microw. Theory Techn.*, vol. 68, no. 8, pp. 1–16, Feb. 2020.
[35] S. C. Cripps, *RF Power Amplifiers for Wireless Communications*, 2nd ed. Norwood, MA, USA: Artech House, 2006, pp. 323–326.
[36] J. Pang, C. Chu, Y. Li, and A. Zhu, "Broadband RF-input continuous-mode load-modulated balanced power amplifier with input phase adjustment," *IEEE Trans. Microw. Theory Techn.*, vol. 68, no. 10, pp. 4466–4478, Oct. 2020.
[37] Innovative Power Products. New York, NY, USA. *Surface Mount 90 Degree Hybrid Couplers*. Accessed: Sep. 15, 2019. [Online]. Available: https://innovativepp.com/product/ipp-7118/
[38] M. Muraguchi, T. Yukitake, and Y. Naito, "Optimum design of 3-dB branch-line couplers using microstrip lines," *IEEE Trans. Microw. Theory Techn.*, vol. MTT-31, pp. 674–678, Aug. 1983.
[39] K. Chen and D. Peroulis, "Design of highly efficient broadband class-E power amplifier using synthesized low-pass matching networks," *IEEE Trans. Microw. Theory Techn.*, vol. 59, no. 12, pp. 3162–3173, Dec. 2011.
[40] P. H. Pednekar, E. Berry, and T. W. Barton, "RF-input load modulated balanced amplifier with octave bandwidth," *IEEE Trans. Microw. Theory Techn.*, vol. 65, no. 12, pp. 5181–5191, Dec. 2017.
[41] A. Barthwal, K. Rawat, and S. K. Koul, "A design strategy for bandwidth enhancement in three-stage Doherty power amplifier with extended dynamic range," *IEEE Trans. Microw. Theory Techn.*, vol. 66, no. 2, pp. 1024–1033, Feb. 2018.
[42] J. Xia, M. Yang, and A. Zhu, "Improved Doherty amplifier design with minimum phase delay in output matching network for wideband application," *IEEE Microw. Wireless Compon. Lett.*, vol. 26, no. 11, pp. 915–917, Nov. 2016.
[43] J. J. M. Rubio, V. Camarchia, M. Pirola, and R. Quaglia, "Design of an 87% fractional bandwidth Doherty power amplifier supported by a simplified bandwidth estimation method," *IEEE Trans. Microw. Theory Techn.*, vol. 66, no. 3, pp. 1319–1327, Mar. 2018.
[44] P. Saad, R. Hou, R. Hellberg, and B. Berglund, "The continuum of load modulation ratio from Doherty to traveling-wave amplifiers," *IEEE Trans. Microw. Theory Techn.*, vol. 67, no. 12, pp. 5101–5113, Dec. 2019.
[45] R. Quaglia and S. Cripps, "A load modulated balanced amplifier for telecom applications," *IEEE Trans. Microw. Theory Techn.*, vol. 66, no. 3, pp. 1328–1338, Mar. 2018.

Yuchen Cao (Graduate Student Member, IEEE) received the bachelor's degree in engineering from Zhejiang University, Hangzhou, Zhejiang, China, in 2011, and the master's degree in electrical engineering from Wichita State University, Wichita, KS, USA, in 2016. He is currently pursuing the Ph.D. degree with the Electrical and Computer Engineering Department, University of Central Florida, Orlando, FL, USA.

He worked as a Mobile Intern Engineer with Qorvo, Apopka, FL, USA, in Summer 2021. His research interests include highly efficient broadband PAs, carrier aggregation, and millimeter-wave circuit design. He was a recipient of the First Place Award of the Student Paper Competition at the IEEE Microwave Theory and Techniques Society (IEEE MTT-S) International Microwave Symposium (IMS) in 2020, the First Place Award of the Student Design Competition on High Efficiency Power Amplifier at IEEE MTT-S IMS in 2020 and 2021, respectively, and the First Place Award of the Student Design Competition on Carrier Aggregation BAW Quadplexer Module at IEEE MTT-S IMS in 2018 and 2019, respectively.

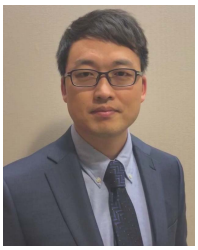

Haifeng Lyu (Graduate Student Member, IEEE) received the bachelor's degree in electrical engineering and automation from the Chengdu University of Technology, Chengdu, Sichuan, China, in 2010, and the master's degree in electrical engineering from the University of Rhode Island, Kingston, RI, USA, in 2017. He is currently pursuing the Ph.D. degree with the University of Central Florida, Orlando, FL, USA.

He was with Qorvo, Apopka, FL, USA, as an RFIC Design Intern, from May 2021 to August 2021. His research interests include novel highly efficient and linear power amplifier (PA) architectures and reconfigurable RF/mm-Wave circuits. He was a recipient of the First Place Award of High Efficiency Power Amplifier Student Design Competition at the IEEE MTT-S International Microwave Symposium (IMS) in 2020 and 2021, consecutively. He was the First Place Winner of Carrier Aggregation BAW Quadplexer Module Design Competition at IMS 2019. He was also the Winner of Second Place Award of Student Paper Competition at IEEE WAMICON 2019.

Kenle Chen (Senior Member, IEEE) received the bachelor's degree in communication engineering from Xi'an Jiaotong University, Xi'an, Shaanxi, China, in 2005, the master's degree in electronics and information engineering from Peking University, Beijing, China, in 2008, and the Ph.D. degree in electrical engineering from Purdue University, West Lafayette, IN, USA, in 2013.

He is currently an Assistant Professor with the Department of Electrical and Computer Engineering, University of Central Florida, Orlando, FL, USA. Before joining UCF in 2018, he was an Assistant Professor with the University of Rhode Island for one year. Prior to his career in academia, he has extensive experiences in wireless and semiconductor industries. From 2015 to 2017, he worked as a Staff RFIC Engineer with Skyworks Solutions, Inc., where he focused on development of RF frontend modules for the advanced smart-phone platforms. From 2013 to 2015, he worked as the Principal/Lead RFIC Engineer with innovational startups, where he led the research and development of multiple successful products of CMOS integrated power amplifiers and frontend solutions for the latest WLAN platforms, such as IEEE802.11ac/ax. As a Graduate Researcher at Purdue University from 2008 to 2013, he made significant contributions in high-efficiency broadband power amplifiers and co-design of reconfigurable RF circuits for smart communication systems. His research interests include energy-efficient, wideband, and ultra-high-speed RF/mm-Wave circuits and systems for 5G-and-beyond communications, extreme-performance power amplifiers in CMOS and compound semiconductor technologies, reconfigurable RF/mm-Wave electronics, and innovational wireless radio concepts/architectures/applications.